Chinese Chemical Letters 36 (2025) 110669

Contents lists available at ScienceDirect

Chinese Chemical Letters

journal homepage: www.elsevier.com/locate/cclet

Modulation of desolvation barriers and inhibition of lithium dendrites based on lithophilic electrolyte additives for lithium metal anode

Qian Wang[a], Dong Yang[b], Wenxing Xin[a], Yongqi Wang[a], Wenchang Han[a], Wengxiang Yan[a], Chunman Yang[a], Fei Wang[c], Yiyong Zhang[a,*], Ziyi Zhu[a,*], Xue Li[a,*]

[a] National local joint engineering research center for Lithium-ion Batteries and Materials Preparation Technology, Key Laboratory of Advanced Batteries Materials of Yunnan Province, Faculty of Metallurgical and Energy Engineering, Kunming University of Science and Technology, Kunming 650093, China
[b] School of Chemistry and Chemical Engineering, Guangxi University, Nanning 530004, China
[c] State Key Laboratory of Chemo/Biosensing and Chemometrics College of Chemistry and Chemical Engineering, Hunan University, Changsha 410082, China

ARTICLE INFO

Article history:
Received 17 October 2024
Revised 14 November 2024
Accepted 21 November 2024
Available online 23 November 2024

Keywords:
Lithium metal anode
Electrolyte additives
Lithophilic metal layer
Lithium ion desolvation
Lithium dendrites

ABSTRACT

Lithium metal has emerged as a highly promising anode material for enhancing the energy density of secondary batteries, attributed to its high theoretical specific capacity and low electrochemical potential. However, safety concerns related to lithium dendrite-induced short circuits and suboptimal electrochemical performance have impeded the commercial viability of lithium metal batteries. Current research efforts primarily focus on altering the solvated structure of Li^+ by modifying the current collector or introducing electrolyte additives to lower the nucleation barrier, expedite the desolvation process, and suppress the growth of lithium dendrites. Nevertheless, an integrated approach that combines the advantages of these two strategies remains elusive. In this study, we successfully employed metal-organic salt additives with lithophilic properties to accelerate the desolvation process, reduce the nucleation barrier of Li^+, and modulate its solvated structure. This approach enhanced the inorganic compound content in the solid electrolyte interphase (SEI) on lithium foil surfaces, leading to stable Li^+ deposition and stripping. Specifically, Li||Cu cells demonstrated excellent cycle life and Coulombic efficiency (97.28% and 98.59%, respectively) at 0.5 mA/cm^2@0.5 mAh/cm^2 and 1 mA/cm^2@1 mAh/cm^2 for 410 and 240 cycles, respectively. Li||Li symmetrical cells showed no short circuit at 1 mA/cm^2@1 mAh/cm^2 for 1150 h, and Li||LFP full cells retained 68.9% of their capacity (104.6 mAh/g) after 250 cycles at N/P (1.1:1.0) with a current density of 1 C.

© 2025 Published by Elsevier B.V. on behalf of Chinese Chemical Society and Institute of Materia Medica, Chinese Academy of Medical Sciences.

In the context of the global energy transition, the advancement of new energy technologies is imperative for fostering a sustainable future [1–3]. With the Paris Agreement establishing clear objectives for global climate action, the development and deployment of alternative energy sources have become increasingly crucial [4,5]. Battery technology, as a pivotal driver of the clean energy revolution, has progressed from lead-acid to lithium-ion batteries [6–10], with each technological advancement significantly enhancing energy density and cycle life. Since the commercialization of Sony's lithium-ion batteries in 1991, these batteries have played a critical role in consumer electronics across various sectors due to their high energy density, high voltage, and lightweight properties. However, the performance of lithium-ion batteries is nearing a plateau in response to growing industry demands, prompting the research community to explore and develop alternative batteries with greater potential [11–17].

In this context, silicon [18–20] and lithium metal [21,22] have emerged as the most promising candidates for next-generation anodes. Among them, lithium-metal batteries are favored for next-generation battery technology due to their excellent theoretical specific capacity (3860 mAh/g) and low electrochemical potential (−3.04 V *vs.* SHE). Compared to traditional graphite anodes, lithium metal anodes can significantly enhance the energy density of batteries, which is critical for meeting future energy demands. Consequently, lithium-based batteries (*e.g.*, lithium-sulfur batteries, Li-Se batteries, Li-O_2 batteries) have been rapidly advancing in recent years [23–27]. However, the commercialization of lithium-metal batteries still faces significant challenges, including lithium dendrite growth, anode volume expansion, and the subsequent rupture of the SEI film, leading to short circuits and thermal run-

* Corresponding authors.
E-mail addresses: zhangyiyong2018@kust.edu.cn (Y. Zhang), zyzhu23@kust.edu.cn (Z. Zhu), Lixue@kust.edu.cn (X. Li).

https://doi.org/10.1016/j.cclet.2024.110669
1001-8417/© 2025 Published by Elsevier B.V. on behalf of Chinese Chemical Society and Institute of Materia Medica, Chinese Academy of Medical Sciences.

away. These issues critically impact the safety and cycle stability of batteries due to electrolyte depletion and “dead lithium” [28–32].

To address these challenges, researchers have been developing various strategies. Huang *et al.* [33]. created a lithophilic layer and a LiF-rich SEI layer on a copper foam skeleton to reduce the Li nucleation barrier and stabilize the SEI. Xu *et al.* [34]. proposed a method involving a multifunctional lithium-pinned array (m-LPA) based on 3D Cu@Cu3P materials, aimed at promoting stable lithium deposition and exfoliation on both the surface and internal structure of 3D copper frameworks. Liu *et al.* [35] used a replacement reaction between $AgNO_3$ and Li to form a lithophilic layer on the Li foil surface, reducing the nucleation barrier. Jia *et al.* [36] formed a porous LiZn alloy coating through an *in situ* reaction between $Zn(TFSI)_2$ and lithium metal to prevent dendrite formation and/or uncontrollable lithium deposition. Fu *et al.* [37] explored a sulfone-based electrolyte containing lithium nitrate ($LiNO_3$), with the addition of 1,1,2,2-tetrafuoroethyl-2,2,2-trifluoroethyl (HFE) to a highly concentrated cyclobutyl sulfone electrolyte, enhancing Li^+ mobility and inhibiting Li dendrite growth. Zhang *et al.* [38,39] developed two innovative approaches based on the double-layer SEI concept, utilizing isosorbide dinitrate (ISDN) and trioxane, respectively, as additives in a locally high-concentration electrolyte (LHCE) to form a dual-layer SEI. This SEI comprises a LiF-enriched bottom layer and a surface layer rich in LiN_xO_y and Li polyoxymethylene, enhancing SEI uniformity and mechanical strength while reducing side reactions between Li and the electrolyte. Zhong *et al.* [40] utilized an ionic liquid additive comprising *N*-methyl-*N*-decyl pyrrolidinium ($Pyr1(10)^+$) cation and bis(trifluoromethanesulphonyl)imide ($TFSI^-$) anion as a non-consumable electrostatic shielding additive, where the long aliphatic chains in the cation "reject Li^+" to form a dense self-healing shielding layer, guiding uniform Li^+ deposition and reducing lithium dendrite formation. Researchers are working on various approaches, including but not limited to collector modification, construction of artificial SEI, and development of electrolyte additives [33–46], to form a stable protective layer on the lithium metal surface to inhibit dendrite growth, mitigate volume expansion, and improve battery performance. Among these, collector modification involves adding a lithophilic layer or artificial SEI layer or constructing a three-dimensional structure on the collector surface to reduce the Li^+ nucleation barrier, alleviate Li volume expansion, and reduce lithium dendrite growth. Electrolyte additive modification focuses primarily on altering the Li^+ solvation structure to reduce the desolvation barrier, accelerate interfacial Li^+ dynamics, or modify the SEI composition through additives to homogenize the SEI and reduce lithium dendrite formation, or expand the electrochemical operating window through additives to achieve lithium-metal batteries with a wide voltage range. However, neither collector modification nor electrolyte additive modification alone can fully address these challenges, warranting further exploration.

In this work, we have thoroughly considered how to combine the advantages of collector modification with those of electrolyte additive modification and explored a simple, no-additional-operation-required battery assembly process to advance the commercial development of lithium metal batteries (LMBs). Taking advantage of the high reactivity of lithium metal and the fast replacement reaction between silver ions, we achieved this by adjusting the ratio of electrolyte additives, accelerating Li^+ desolvation, guiding uniform Li^+ deposition, and modifying the SEI composition of the Li foil surface. And the addition of this additive regulates the Li^+ solvation structure, so that more organic anions ($TFSI^-$) regulate the SEI composition on the Li foil surface, and more inorganic components to enhance the mechanical properties of the SEI, which alleviates the lithium dendrites problem in lithium metal anode batteries (LMAs) during deposition and stripping (Fig. 1). As a result, Li||Cu cells based on a silver-containing lithophilic layer (AgTFSI) demonstrated excellent performance at 0.5 mA/cm^2@0.5 mAh/cm^2, and 1 mA/cm^2@1 mAh/cm^2 for the 410th and 240th cycles, respectively, with a Coulombic efficiency (hereinafter referred to as CE) of 97.28% and 98.59%. The Li||Li symmetric cells exhibited a cycle life of 1150 h at a current density of 1 mA/cm^2 and a lithium metal deposition of 1 mAh/cm^2. Lithium foil with $LiFePO_4$ cathode full cells (Li||LFP cells) assembled using AgTFSI additives also maintained good discharge-specific capacity, cycle life, and rate performance.

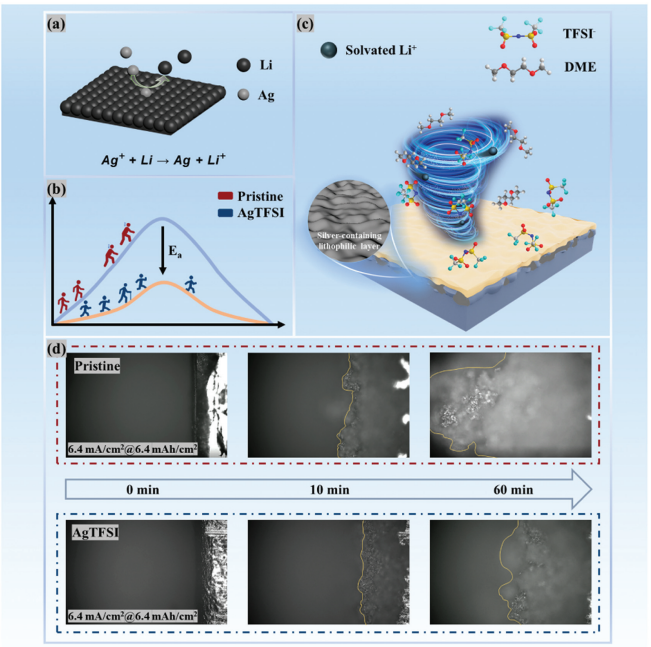

Fig. 1. Mechanism diagram of (a) high reactivity of Li metal and Ag^+ displacement reaction. (b) Introduction of AgTFSI to lower the Li^+ desolvation potential. (c) The silver-containing lithophilic layer accelerates the desolvation of solvated Li^+ and alters the solvated structure of Li^+. (d) At 6.4 mA/cm^2@6.4 mAh/cm^2 conditions, *in-situ* optical microscopy was used to observe lithium metal deposition from the Pristine electrolyte and the AgTFSI electrolyte.

After examining the presence of silver metal on the surface of lithium metal at various ratios and testing the performance of Li||Cu cells (Fig. S1 in Supporting information), 0.5% AgTFSI (hereafter referred to as AgTFSI) was identified as the optimal choice. To demonstrate that anodes treated with AgTFSI electrolyte exhibit a lithophilic silver layer on their surface, the AgTFSI anodes were analyzed using X-ray diffraction (XRD), X-ray photoelectron spectroscopy (XPS), and scanning electron microscope & energy dispersive spectroscopy (SEM&EDS) (Figs. 2a-e). The formation of the lithophilic silver layer *via* a substitution reaction was confirmed by XRD and XPS (Figs. 2a and b). The XRD pattern of the AgTFSI anode displayed four characteristic peaks corresponding to metallic silver at $2\theta = 38.116°$, 44.227°, 64.98°, and 76.66°, which we attribute to the high reactivity of lithium metal and the lithophilicity of silver metal, resulting in the partial formation of a silver-lithium alloy layer (Fig. 2a). Additionally, the XPS spectrum of the AgTFSI anode (Fig. 2b) revealed two characteristic peaks at 373.65 and 367.63 eV, corresponding to the binding energies of Ag $3d_{3/2}$ and Ag $3d_{5/2}$, respectively, with an inter-peak spacing of 6.02 eV, confirming the presence of metallic silver. In contrast to the smooth surface of bare Li foil (Fig. S2 in Supporting information), SEM images of the AgTFSI anode (Figs. 2c and d) clearly show a hilly, zone-like surface, indicative of silver metal. The morphology of this surface suggests the presence of more lithophilic active sites, which could effectively guide the uniform and dense deposition of Li^+.

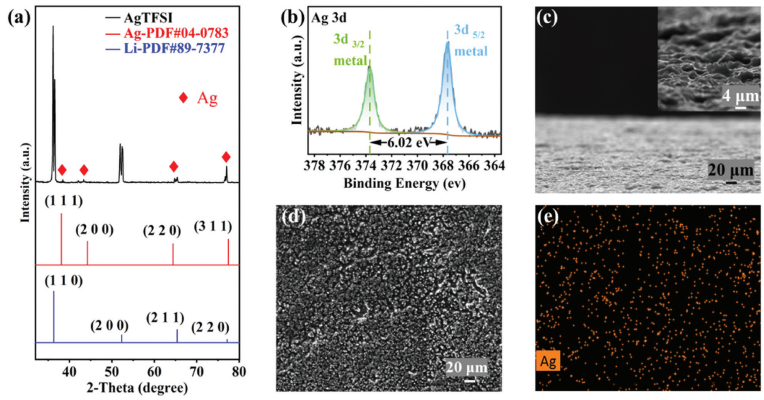

Fig. 2. (a) XRD patterns of Ag-modified Li anodes before cycling. (b) Ag 3d XPS spectra of AgTFSI anodes before cycling. SEM image of AgTFSI anodes (c) cross-section and (d) surface before cycling. (e) Corresponding EDS mapping of Ag.

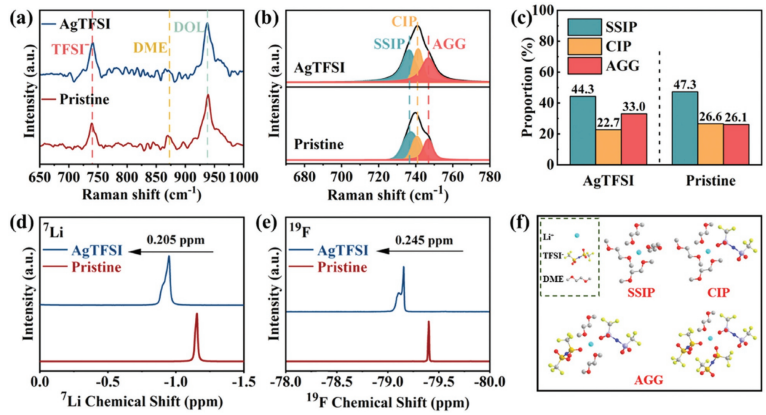

Fig. 3. (a) Raman spectra of the corresponding electrolyte. (b) Peak fitting of $TFSI^-$ and (c) concretization. (d) ^7Li and (e) ^{19}F NMR spectra of AgTFSI and Pristine. (f) Schematic diagram of Li^+ solvation structure.

As indicated by SEM-EDS in Fig. 2e, there is a uniform distribution of metallic silver on the surface of lithium metal.

To elucidate the behavior of AgTFSI within the electrolyte, the solvated structure of Li^+ was investigated using Raman spectroscopy. As depicted in Fig. 3a, the spectral region between 720 cm^{-1} and 760 cm^{-1} corresponds to the vibrational signal peaks of S-N-S and C-S bonds within $TFSI^-$, where the S-N-S bending frequency shifts due to interactions with Li^+. Additionally, the DME molecular vibration peaks were observed in the range of 800–880 cm^{-1}, with the peaks at 825 and 850 cm^{-1} corresponding to the bending vibration of -CH_2 and the stretching vibration of C–O in the DME molecule, respectively. Compared to the Pristine electrolyte, the DME molecular vibration peak intensity in the AgTFSI electrolyte increased, indicating a higher number of free DME molecules. Further Raman spectral fitting in the range of 670–780 cm^{-1} was conducted to determine the relative proportions of different solvated clusters (Fig. 3b). Unique peaks representing solvated TFSI-ligand complexes were identified between 720 cm^{-1} and 760 cm^{-1}. The introduction of the metal-organic salt AgTFSI prompted TFSI- to participate in the solvated structure of Li^+, forming more ionic aggregates (AGG). The proportions of SSIP (737 cm^{-1}) and CIP (741 cm^{-1}) decreased from 47.3% and 26.6% to 44.3% and 22.7%, respectively, while AGG (747 cm^{-1}) increased from 26.1% to 33.0% (Figs. 3c-f).

To corroborate these findings, nuclear magnetic resonance (NMR) tests were performed. The NMR results revealed notable chemical shifts in both the ^7Li (Fig. 3d) and ^{19}F (Fig. 3e) spectra (0.205 and 0.245 ppm, respectively) towards lower fields following the addition of the AgTFSI electrolyte additive. This suggests that the interactions between Li^+ and solvent molecules were weakened, while the ionic coordination between Li^+ and $TFSI^-$ was strengthened. Together, Raman spectroscopy and NMR analysis confirmed that the addition of the organometallic salt AgTFSI effectively reduces the coordination degree of DME molecules and alters the original solvated structure of Li^+. This coordination is replaced by the interaction between $TFSI^-$ and Li^+, facilitating the decomposition of $TFSI^-$ at the SEI interface and generating more inorganic components with high mechanical strength, thereby enhancing the stability of the SEI.

Linear scanning voltammetry (LSV) measurements were performed using a Li||Li symmetric cell with the specified electrolyte (Fig. 4a). The resulting exchange current density (i_0) was fitted according to Eq. S1 (Supporting information), revealing the i_0 value for the Pristine electrolyte is 2.151 mA/cm^2, while the higher i_0 value for the AgTFSI electrolyte (2.675 mA/cm^2) indicates faster ion migration at the interface. As shown in Fig. 4b, the lithium nucleation overpotential on the Cu collector substrate was measured using cyclic voltammetry (CV) to further elucidate the ion transfer kinetics. The overpotential of the Pristine electrolyte is 40 mV, while the overpotential of the AgTFSI electrolyte is 18 mV lower, indicating accelerated charge transfer kinetics. The silver-containing lithium layer effectively reduces the nucleation barrier. To confirm the stability of AgTFSI in the electrolyte, LSV testing showed that its oxidation window is wider than its electrochemical stability window, indicating its stable existence (Fig. 4c). Furthermore, Li||Li symmetric cells were assembled and subjected to impedance

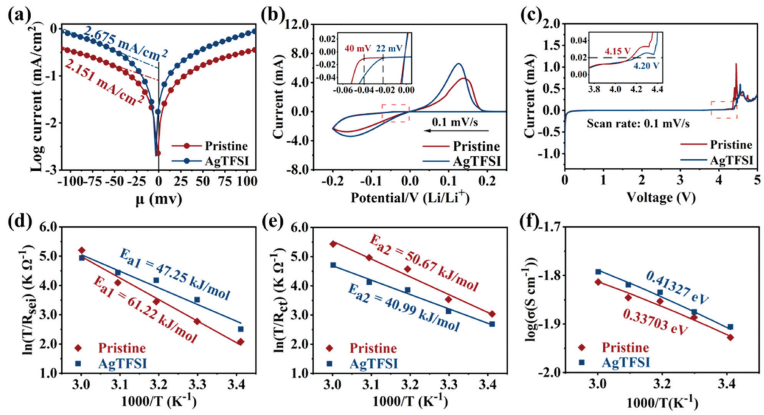

Fig. 4. (a) Tafel plots derived from Li||Li symmetric cells using the Pristine electrolyte and AgTFSI electrolyte. (b) Cycling voltammograms of Li||Cu cells for the Pristine electrolyte and AgTFSI electrolyte, recorded at a scan rate of 0.1 mV/s within a voltage range of −0.25~0.25 V. (c) Linear sweep voltammograms of the Pristine electrolyte and AgTFSI electrolyte conducted at a scan rate of 0.1 mV/s. Plotting the natural logarithm of overpotential for constant current Li^+ deposition/stripping against current density and activation energies (d) R_{sei} and (e) R_{ct} obtained from Nyquist plots of cyclic Li||Li cells using the Pristine electrolyte and AgTFSI electrolyte at various temperatures. (f) Relationship between temperature and ionic conductivity for the Pristine electrolyte and AgTFSI electrolyte.

testing across a temperature range of 20–60 °C after 10 deposition/stripping cycles at a current density of 1 mA/cm^2 and a deposition amount of 1 mAh/cm^2. The results showed a decreasing trend in impedance values with increasing temperature, indicating temperature-dependent changes (Fig. S3 in Supporting information). The activation energy (E_a) was subsequently calculated using the Arrhenius equation through a linear fit of impedance *versus* temperature (Eq. S2 in Supporting information). Linear regression analysis (Tables S1 and S2 in Supporting information) of T^{-1} *versus* lnR_1 (representing SEI resistance) and lnR_2 (representing charge transfer resistance) yielded E_{a1} and E_{a2}. Among these, E_{a1} represents the potential barrier for the migration and diffusion of Li^+ in the SEI, while E_{a2} represents the energy required for Li^+ release and dissociation in the solvation layer. The E_{a1} value for Li^+ migration in the SEI of the AgTFSI electrolyte (47.25 kJ/mol) is lower than that of the Pristine electrolyte (61.22 kJ/mol) (Fig. 4d), and the E_{a2} value for Li^+ desolvation capacity (40.99 kJ/mol) exhibited a similar trend when compared to the Pristine electrolyte (50.67 kJ/mol) (Fig. 4e). We infer that the uneven morphology of the silver-containing lithophilic layer in AgTFSI could provide more nucleophilic sites, reducing the nucleation barrier for lithium, promoting the solvation-desolvation process of Li^+, and facilitating rapid Li^+ diffusion at the interface through SEI regulation. Additionally, by investigating the temperature-dependent changes in ionic conductivity of the Pristine and AgTFSI electrolytes (20–60 °C) (Fig. S4 in Supporting information) and analyzing the nonlinear relationship between electrolyte logσ and T^{-1} using the Vogel-Fulcher-Tamman (VFT) equation (Eq. S3 and Table S3 in Supporting information), it was found that the E_a value of the AgTFSI electrolyte (0.41327 eV) is higher than that of the pristine electrolyte (0.33703 eV) (Fig. 4f), likely due to the increased involvement of $TFSI^-$ anions in the solvation structure of Li^+. This leads to the formation of ionic aggregates that hinder rapid ion movement within the electrolyte. However, these aggregates may promote anion decomposition, resulting in the formation of an SEI rich in inorganic compounds on the anode surface, thereby improving the mechanical strength of the SEI and inhibiting lithium dendrite growth.

The morphology of lithium deposition after cycling with Pristine electrolyte and AgTFSI electrolyte was characterized by scanning electron microscopy (SEM). As depicted in Fig. 5a, the lithium metal layer with Pristine electrolyte exhibited a cracked and large morphological organization. The cross-sectional view (Fig. 5c) further reveals that the lithium metal deposition layer in the Pristine electrolyte shows a fractured and uneven morphology. This phenomenon is attributed to side reactions within the electrolyte and the non-uniform deposition of lithium, leading to the formation of inactive lithium (dead lithium) that easily detaches from the larger lithium deposits. This detachment results in low CE and a shortened cycle life for batteries utilizing Pristine electrolyte. In contrast, the AgTFSI electrolyte, which forms a lithophilic silver layer, provides more nucleation sites, resulting in a lithium metal layer that is densely organized, flat, and uniformly distributed (Fig. 5b). The cross-sectional view of the AgTFSI electrolyte (Fig. 5d) demonstrates a significantly different, more densely and uniformly organized lithium metal deposition layer compared to the Pristine electrolyte. To further investigate, *in-situ* observation of the Li^+ deposition process was conducted using an optical microscope at 6.4 mA/cm^2@6.4 mAh/cm^2 (Fig. 1). Results showed that prominent lithium dendrites and uneven lithium deposition appeared after 10 min with Pristine electrolyte. However, with AgTFSI electrolyte, the growth of lithium dendrites during the Li^+ deposition/stripping process was effectively mitigated, demonstrating the key role of the silver-containing lithophilic layer in stabilizing lithium metal deposition.

X-ray photoelectron spectroscopy (XPS) was utilized to investigate the chemical composition of the SEI formed on the surface of Li foil, with lithium metal anodes etched at varying depths (Fig. S5 in Supporting information). The Ag 3d spectra (Fig. 5e) confirmed the presence of a silver-containing lithophilic layer throughout the SEI region, which enhances Li^+ diffusive migration and reduces the potential barriers for Li^+ desolvation, thus accelerating interfacial dynamics on lithium-metal surfaces. SEI analysis (Fig. S6 in Supporting information) revealed carbonaceous decomposition by-products in the C 1s spectra, including C=C, C–O–C, C=O, and O–C=O, located at 284.8, 286.6, 288.6, and 289.8 eV, respectively. Examination of the Li 1s spectra (Figs. 5f and g) showed significant compositional differences in the SEI composition distribution between Pristine and AgTFSI modified electrolyte. The SEI layer formed with AgTFSI electrolyte demonstrated consistent component distribution across etching depths, whereas the Pristine electrolyte exhibited considerable variation, particularly in LiF peaks. This suggests that the SEI formed in the Pristine electrolyte is uneven, which may compromise its chemical and mechanical strength, promote the growth of lithium dendrites, and result in a shorter cycle life and lower CE. In contrast, the SEI formed by the AgTFSI electrolyte is uniformly composed of inorganic and organic substances, exhibiting superior overall strength. This uniform SEI effectively isolates the lithium metal anode from the electrolyte,

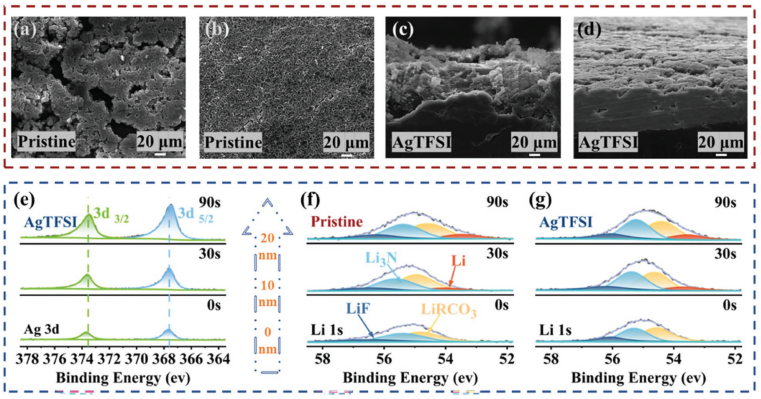

Fig. 5. The SEM images of Pristine electrolyte and AgTFSI electrolyte Li||Li symmetric cells after 30 cycles at 1 mA/cm^2@1 mAh/cm^2: (a-d) surface and cross-section. X-ray photon spectroscopy (XPS) of lithium metal negative electrode at different etching depths (0, 10, 20 nm) compared with Pristine electrolyte and AgTFSI electrolyte: (e) Ag 3d XPS spectra, (f, g) Li 1s XPS spectra.

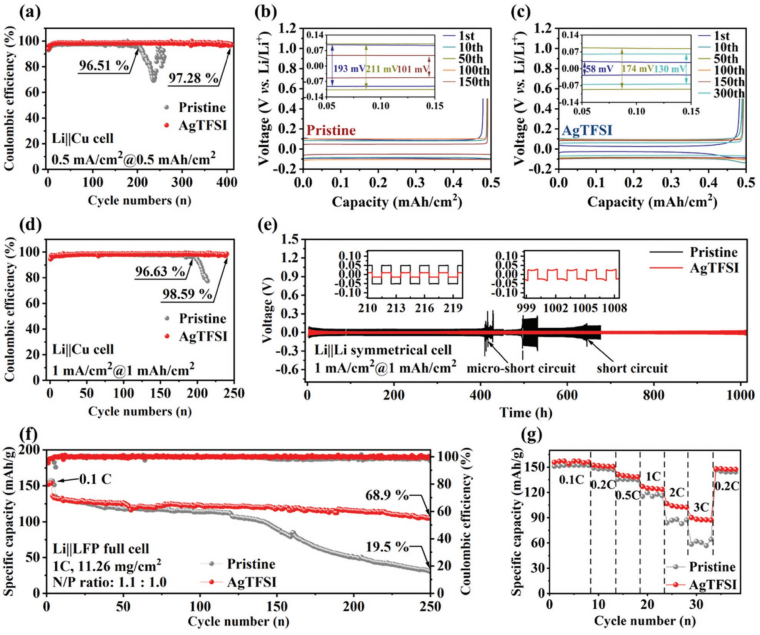

Fig. 6. Cycle performance of different electrolyte Li||Cu cells: (a) at 0.5 mA/cm^2@0.5 mAh/cm^2. Regarding the capacity voltage diagram of (b) Pristine electrolyte and (c) AgTFSI electrolyte. (d) Cycle performance of different electrolyte Li||Cu cells at 1 mA/cm^2@1 mAh/cm^2. (e) Cycle performance of different electrolyte Li||Li symmetrical cells at 1 mA/cm^2@1 mAh/cm^2. Li||LFP full cells at NP ratio = 1.1:1.0. (f) Cycling performance at 1 C and (g) rate performance.

minimizes harmful side reactions, and enables more stable battery operation. Furthermore, the F 1s spectra (Fig. S7 in Supporting information) showed that the Li foil with AgTFSI electrolyte exhibits almost no C–F component in the 20 nm region (90 s). This is attributed to the fact that the AgTFSI organometallic additive altered the solvated structure of Li^+ and accelerated Li^+ desolvation, with $TFSI^-$ participating in the solvated Li^+ structure, leading to the formation of LiF degradation products on the Li foil.

The cycle life and CE of the batteries were assessed by assembling Li||Cu and Li||Li symmetric cells to evaluate the protective performance of the lithium metal anode. The Li||Cu cell with pristine electrolyte at 0.5 mA/cm^2@0.5 mAh/cm^2 exhibited a limited cycle life of 200 cycles with a CE of 96.51%. In contrast, AgTFSI demonstrated a significantly improved cycle life exceeding 410 cycles with CE of 97.28% (Fig. 6a). As shown in Figs. 6b and c, overpotential analysis in Li||Cu cells indicated that the first-cycle overpotential for AgTFSI (58 mV) was much lower than that of the Pristine electrolyte (193 mV). Furthermore, the overpotential of AgTFSI consistently remained consistently lower than that of the pristine electrolyte during cycling. This improvement is likely attributed to the silver-containing lithium layer in AgTFSI, which offers more nucleation sites and results in a more uniform SEI composition, effectively lowering the nucleation barrier of lithium. As shown in Fig. 6d, Li||Cu cells at 1 mA/cm^2@1 mAh/cm^2 displayed a similar trend, The cycle life of AgTFSI exceeds that of CE stable at 98.59% after 240 cycles, while the Pristine electrolyte showed significant efficiency degradation after 195 cycles, inferred to result from the uncontrollable, non-uniform growth of lithium dendrites during Li^+ deposition/stripping, leading to dendrites piercing the separator and causing a short circuit. Furthermore, the advantage of AgTFSI became even more apparent at varying current densities (Fig. S8 in Supporting information). Li||Cu cells at 0.5 mA/cm^2@1 mAh/cm^2, 1 mA/cm^2@2 mAh/cm^2, and 2 mA/cm^2@1 mAh/cm^2 consistently exhibited superior cycle life with AgTFSI compared to the Pristine electrolyte. This supports the hypothesis that the addition of AgTFSI forms a silver-containing lithophilic layer, which lowers the nucleation barrier and alters the solvated structure of Li^+, resulting in an SEI with more stable properties. The cycle life was

further analyzed using Li||Li symmetric cells (Fig. 6e and Fig. S9 in Supporting information). At 1 mA/cm^2@1 mAh/cm^2 (Fig. 6e), the pristine electrolyte showed unstable cycle life, with potential micro-short circuits occurring around 400 h due to lithium dendrites puncturing the separator. In contrast, AgTFSI exhibited excellent cycle life, exceeding 1000 h Analysis of the enlarged time-voltage profile during a specific period (Fig. 6e) revealed that the polarization potential of the pristine electrolyte was significantly higher than that of AgTFSI. Similar electrochemical performance was observed at current densities of 0.5 and 2 mA/cm^2 (details in Fig. S9), which we attribute to the lithophilicity of the silver layer and the enhanced participation of $TFSI^-$ in the Li^+ solvation structure with AgTFSI, optimizing the potential barrier during Li^+ deposition/stripping. This leads to a more uniform and stable SEI composition on the Li foil, subsequently extending its stabilization and cycle life.

To evaluate the applicability of AgTFSI electrolyte for lithium metal anode protection across various applications, Li||LFP full cells were assembled for electrochemical performance testing. The electrochemical performance of Li||LFP full cells with an N/P ratio of 1.1:1.0 is shown in Figs. 6f and g, Figs. S10 and S11 (Supporting information). The cells were activated at a current density of 0.1 C (1 C = 170 mAh/g) for the first three cycles. At a current density of 1 C, AgTFSI exhibited a significantly better cycle life than the pristine electrolyte. After 250 cycles, the capacity of AgTFSI (104.6 mAh/g) was substantially higher than that of the pristine electrolyte (30.3 mAh/g), with respective capacity retention rates of 68.9% and 19.5%. The average capacity decay rate per cycle was 0.124% for AgTFSI electrolyte and 0.322% for the pristine electrolyte (Fig. 6f). Furthermore, the Li||LFP full cell assembled with AgTFSI electrolyte showed good cycle life, with 66.8% capacity retention after 225 cycles at a current density of 0.5 C. As seen in the magnification performance test results in Fig. 6g, AgTFSI maintained higher capacity at higher rates.

Moreover, lithium metal-sulfur cells (Li||S cells) matched with sulfur cathodes were also assembled for electrochemical performance tests (Fig. S11). It was found that AgTFSI electrolyte continued to exhibit good electrochemical performance in Li||S cells. Therefore, the stable lithophilic layer containing metallic silver enhances the electrochemical performance of full cells. We infer that the addition of AgTFSI reduces the nucleation and diffusion barriers of Li^+, leading to improved performance.

In conclusion, we have demonstrated the advantages of combining collector modification with electrolyte additive modification by introducing an organometallic salt additive containing lithophilic metal cations to stabilize Li^+ deposition/stripping *via* a silver-containing lithophilic interface. Leveraging the high reactivity of lithium metal, a finely organized and uniform lithophilic interfacial layer with a hilly zone-like morphology is formed through a substitution reaction on the surface of the lithium metal collector, providing additional nucleation sites for lithium deposition. This unique hilly-ribbon-like structure effectively reduces the nucleation barrier of lithium, accelerates the desolvation of Li^+, and alters its solvated coordination structure. The formation of an SEI rich in inorganic compounds and a lithophilic silver layer effectively addresses the challenge of inhibiting lithium dendrite growth, thus stabilizing the Li^+ deposition/stripping process. Using this bifunctional electrolyte additive, Li||Cu cells achieved impressive cycling performances of 410 and 240 cycles at current densities of 0.5 and 1 mA/cm^2, respectively, while Li||Li symmetric cells maintained stability over 1150 h at a current density of 1 mA/cm^2@1 mAh/cm^2. Furthermore, the effectiveness of this electrolyte additive was validated in Li||LFP full cells (N/P = 1.1:1.0) and Li||S cells. The simplicity of this assembly process, which requires no additional complex operations, holds great promise for accelerating the commercial development of lithium-metal batteries.

Declaration of competing interests

The authors declare that they have no known competing financial interests or personal relationships that could have appeared to influence the work reported in this paper.

CRediT authorship contribution statement

Qian Wang: Writing – original draft, Methodology, Investigation, Data curation. **Dong Yang:** Methodology, Investigation, Data curation. **Wenxing Xin:** Validation, Investigation. **Yongqi Wang:** Validation, Methodology, Investigation. **Wenchang Han:** Validation, Methodology, Investigation. **Wengxiang Yan:** Writing – review & editing. **Chunman Yang:** Writing – review & editing. **Fei Wang:** Writing – review & editing, Conceptualization. **Yiyong Zhang:** Writing – review & editing, Supervision, Funding acquisition. **Ziyi Zhu:** Writing – review & editing, Conceptualization. **Xue Li:** Supervision, Formal analysis.

Acknowledgments

This work was financially supported by Yunnan Natural Science Foundation Project (No. 202202AG050003), Yunnan Fundamental Research Projects (Nos. 202101BE070001-018 and 202201AT070070), the National Youth Talent Support Program of Yunnan Province China (No. YNQR-QNRC-2020-011), Yunnan Engineering Research Center Innovation Ability Construction and Enhancement Projects (No. 2023-XMDJ-00617107).

Supplementary materials

Supplementary material associated with this article can be found, in the online version, at doi:10.1016/j.cclet.2024.110669.

References

[1] A.S. Mohd Razif, N.F. Ab Aziz, M.Z.A. Ab Kadir, K. Kamil, Energy Strat. Rev. 52 (2024) 101346.
[2] C. Zhang, Y. Yang, X. Liu, et al., Innovation 4 (2023) 100518.
[3] P. Greim, A.A. Solomon, C. Breyer, Nat. Commun. 11 (2020) 11.
[4] J.A. Lowe, D. Bernie, Philos. T. R. Soc. A 376 (2018) 20170263.
[5] D. Mitchell, M.R. Allen, J.W. Hall, et al., Philos. T. R. Soc. A 376 (2018) 20180066.
[6] G.N. Lewis, F.G. Keyes, J. Am. Chem. Soc. 35 (1913) 340–344.
[7] M. Armand, J.M. Tarascon, Nature 451 (2008) 652–657.
[8] D.D. Sarma, A.K. Shukla, ACS Energy Lett. 3 (2018) 2841–2845.
[9] P.P. Lopes, V.R. Stamenkovic, Science 369 (2020) 923–924.
[10] D.T. Wrublewski, Sci. Technol. Libr. 39 (2020) 51–67.
[11] Y.K. Sun, ACS Energy Lett. 2 (2017) 2694–2695.
[12] X.Q. Zhang, C.Z. Zhao, J.Q. Huang, Q. Zhang, Engineering 4 (2018) 831–847.
[13] F.X. Wu, J. Maier, Y. Yu, Chem. Soc. Rev. 49 (2020) 1569–1614.
[14] C. Xu, K. Zhang, D. Zhang, et al., Nano Energy 68 (2020) 104318.
[15] X. Yang, F. Su, M. Hou, et al., Dalton Trans. 50 (2021) 7041–7047.
[16] Z. Yao, Y. Kang, M. Hou, et al., Adv. Funct. Mater. 32 (2022) 2111919.
[17] S. Xin, X. Zhang, L. Wang, et al., Sci. China Chem. 67 (2024) 13–42.
[18] M.N. Obrovac, Curr. Opin. Electrochem. 9 (2018) 8–17.
[19] Z.Y. Feng, W.J. Peng, Z.X. Wang, et al., Int. J. Miner. Metall. Mater. 28 (2021) 1549–1564.
[20] X. Lei, Y. Wang, J. Wang, et al., Small Methods 8 (2024) 2300754.
[21] Y. Zhang, T.T. Zuo, J. Popovic, et al., Mater. Today 33 (2020) 56–74.
[22] M. Qi, L. Xie, Q. Han, et al., J. Energy Storage 47 (2022) 103641.
[23] Q.J. Shao, S.D. Zhu, J. Chen, Nano Res. 16 (2023) 8097–8138.
[24] C.M. Yang, F. Wang, D. You, et al., Chem. Eng. J. 496 (2024) 153812.
[25] J. Liu, F. Wang, H. Wei, et al., Chin. Chem. Lett. (2024), doi:10.1016/j.cclet.2024.110475.
[26] P. Xu, X. Lin, Z. Sun, et al., J. Energy Chem. 72 (2022) 186–194.
[27] S.S.H. Zaidi, X. Li, Adv. Energy Mater. 13 (2023) 2300985.
[28] R. Bhattacharyya, B. Key, H. Chen, et al., Nat. Mater. 9 (2010) 504–510.
[29] S. Chandrashekar, N.M. Trease, H.J. Chang, et al., Nat. Mater. 11 (2012) 311–315.
[30] D. Lu, Y. Shao, T. Lozano, et al., Adv. Energy Mater. 5 (2015) 1400993.
[31] K.N. Wood, E. Kazyak, A.F. Chadwick, et al., ACS Cent. Sci. 2 (2016) 790–801.
[32] X.Q. Xu, X.B. Cheng, F.N. Jiang, et al., SusMat 2 (2022) 435–444.
[33] K. Huang, S. Song, Z. Xue, et al., Energy Storage Mater. 55 (2023) 301–311.
[34] P. Xu, X. Lin, X. Hu, et al., Energy Storage Mater. 28 (2020) 188–195.
[35] T. Liu, Q. Hu, X. Li, et al., J. Mater. Chem. A 7 (2019) 20911–20918.
[36] Z. Jia, H. Lyu, W. Wang, et al., J. Alloys Compd. 936 (2023) 168108.
[37] J. Fu, X. Ji, J. Chen, et al., Angew. Chem. Int. Ed. 59 (2020) 22194–22201.

[38] Q.K. Zhang, S.Y. Sun, M.Y. Zhou, et al., Angew. Chem. Int. Ed. 62 (2023) e202306889.
[39] Q.K. Zhang, X.Q. Zhang, J. Wan, et al., Nat. Energy 8 (2023) 725–735.
[40] J. Zhong, Z.X. Wang, S.W. Wang, et al., Appl. Surf. Sci. 622 (2023) 156968.
[41] W. Liu, P. Liu, D. Mitlin, Adv. Energy Mater. 10 (2020) 2002297.
[42] U. Pal, D. Rakov, B.Y. Lu, et al., Energy Environ. Sci. 15 (2022) 1907–1919.
[43] F. Zhao, P. Zhai, Y. Wei, et al., Adv. Sci. 9 (2022) 2103930.
[44] D. Yang, X. Wang, Q. Wang, et al., Energy Storage Mater. 72 (2024) 103719.
[45] Z. Wang, L.P. Hou, Q.K. Zhang, et al., Chin. Chem. Lett. 35 (2024) 108570.
[46] Q. Zhang, S. Liu, Z. Lin, et al., Nano Energy 74 (2020) 104860.